Biosensors and Bioelectronics 137 (2019) 154–160

Contents lists available at ScienceDirect

Biosensors and Bioelectronics

journal homepage: www.elsevier.com/locate/bios

Enhanced 3D paper-based devices with a personal glucose meter for highly sensitive and portable biosensing of silver ion

Wencheng Xiao, Yiming Gao, Yun Zhang*, Jiao Li, Zhaoying Liu, Jinfang Nie**, Jianping Li

College of Chemistry and Bioengineering, Guilin University of Technology, Guilin, 541004, PR China

ARTICLE INFO

Keywords:
Paper-based microfluidics
Signal amplification
Point-of-care biosensor
Glucometer
Ag^+

ABSTRACT

A variety of routine methods are available for the detection of silver (I) (Ag^+) ions, but most of them rely on expensive, sophisticated and desktop instruments. Herein, a low-cost, instrument-free and portable Ag^+ biosensor was described by initially designing a new class of 3D origami microfluidic paper-based analytical devices (μPADs) into each of which one piece of reagent-loaded nanoporous membrane was integrated. It combines analyte-triggered self-growing of silver nanoparticles to block the membrane's pores in situ for rapid yet efficient signal amplification with a handheld personal glucose meter for a portable and sensitive quantitative readout based on the biocatalytic reactions between the glucose oxidase and glucose. Its utility is well demonstrated with the specific detection of the analyte with a limit of detection as low as ~58.1 pM (3σ), which makes this new biosensing method one of the most sensitive Ag^+ assays in comparison with many other typical methods recently reported. Moreover, the satisfactory recovery of analyzing several types of real water examples, i.e., tap water, drinking water, pond water and soil water, additionally validates its feasibility for practical applications.

1. Introduction

Heavy metals are generally defined as metals with atomic weights in the range of 63.5–200.6 g M^{-1} and a specific gravity higher than 5 g cm^{-3} (Gumpu et al., 2015). These substances are among the most harmful environmental pollutants as they are non-biodegradable and can accumulate in ecological systems (Lin et al., 2016). In case of food chain systems, they will lead to food contamination which can eventually do irreversible damage to the human body and cause various diseases (Dai et al., 2012; Lin et al., 2016; Yang and Wang, 2011). For instance, silver (I) (Ag^+) ion is part of the largest toxicity class of heavy metal pollutants (Ratte, 1999). According to the US Environmental Protection Agency, the Ag^+ will show toxicity to fishes and microorganisms if its concentrations are above 1.6 nM, and its maximum allowable level in drinking water is strictly limited to 900 nM (Alizadeh et al., 2014). The Ag^+ can not only inactivate enzymes by binding to thiol, amino, and carboxyl groups (Drake and Hazelwood, 2005; Gao et al., 2017; Hadrup and Lam, 2014), but also damage DNAs via formation of Ag^+-polynucleotide complexes (Choi et al., 2016; Hossain and Huq, 2002). In fact, excessive intake of Ag^+ could result in argyria and severe symptoms including a headache, stomach distress, organ oedema, or even death (Kumar et al., 2011; Miao et al., 2013). Thus, highly sensitive and specific methods to detect Ag^+ are of great importance for environmental protection and water safety.

Traditional routine techniques for this goal include atomic absorption and emission spectrometry (Trindade et al., 2015), inductively coupled plasma mass spectrometry (Wang et al., 2015), and ion-selective electrodes (Mensah et al., 2014). A series of new Ag^+ assay approaches have also been developed in recent years, such as fluorescence spectrometry (with Al_2O_3 nanoparticles@Au nanodot (Chen et al., 2013), trinuclear gold(I) pyrazolate (Upadhyay et al., 2018) or fluorescent protein (Chen et al., 2018) probes), surface plasmon resonance (Chang et al., 2012), absorption spectrometry (using polyvinylpyrrolidone-capped Pt cubes as colorimetric probes (Gao et al., 2017)), and electrochemical sensors based on enzyme cleavage (Miao et al., 2013). These analytical methods have their own unique advantages and can offer satisfactory sensitivity and specificity. However, most of them are not suited for point-of-care testing (POCT) uses in resource-limited settings (e.g., the field-based analysis in remote regions and home healthcare), as they are tedious (typically 0.5–1 h) and generally require expensive, bulky instruments and well-trained operators.

Microfluidic paper-based analytical devices (μPADs), first described by Whitesides and co-workers in 2007 (Martinez et al., 2007; Yamada et al., 2015), possess many attractive features (Lin et al., 2016; Morbioli et al., 2017; Nie et al., 2012; Xia et al., 2016; Yang et al., 2016; Zhang

* Corresponding author.
** Corresponding author.
E-mail addresses: zy@glut.edu.cn (Y. Zhang), Niejinfang@glut.edu.cn (J. Nie).

https://doi.org/10.1016/j.bios.2019.05.003
Received 14 December 2018; Received in revised form 20 April 2019; Accepted 2 May 2019
Available online 06 May 2019
0956-5663/

et al., 2016) and may provide promising alternative platforms for designing POCT Ag^+ assays. The μPAD's primary features include the extremely low cost of materials, ease of device fabrication and use, portability, and disposability. Moreover, it consumes quite small volumes of reagent and sample (typically several microliters in an assay), and has the ability to function via capillary action (without using an external mechanical or electrical fluid-driving pump). As a result, the last decade has witnessed fast progress in the fabrications of various 2D and 3D μPADs for inexpensive, portable detection of a wide range of analytes (e.g., ions, small molecules, proteins, DNAs, and even cancer cells) (Lin et al., 2016; Morbioli et al., 2017; Xia et al., 2016; Yang et al., 2016). There are only a few of paper-based Ag^+ assay methods previously proposed. For example, in the study by Yang and Wang (2011), naked-eye detection of Ag^+ was conducted in test paper under UV light through the reduction of *o*-phenylenediamine by the analyte producing a fluorescent derivative. Lin's group (Liu and Lin, 2014) and Hossain's group (Hossain and Brennan, 2011) prepared two types of target-specific-indicator-loaded test paper strips for colourimetric Ag^+ sensing. Nevertheless, these paper-based systems disclosed to date either needed precise yet tedious control of temperatures to realize a qualitative analysis of nanomolar Ag^+ or had to use a scanner or camera to quantitatively get micromolar detection limits. Currently, it still remains a significant challenge to develop equipment-free quantitative paper-based assays that enable the detection of Ag^+ at nanomolar or lower levels and could meet an increasing demand for POCT water monitoring by limitedly-trained personnel or even unskilled home-users.

In this work, we respond to this challenge by describing the proof-of-concept of a complementary paper-based Ag^+ assay, using analyte-triggered self-growing reactions in 3D origami nanoporous-membrane-integrated μPADs (NM-μPADs) for rapid signal amplification and a ubiquitous personal glucose meter (PGM) as a quantitative signal reader. Battery-powered handheld PGMs are one family of portable biosensors during the most successful POCT sensors worldwide. Their wide success is largely due to low price, 'pocket' size, simple operation, and highly sensitive signal measurement via the biocatalytic reactions between glucose oxidase and glucose (Xiang and Lu, 2011). Inspired by these noticeable analytical advantages, although the current state-of-art PGMs can only detect a single target, glucose (Xiang and Lu, 2012), some efforts have been devoted in recent years to realize PGM-based POCT detection of various non-glucose targets ranging from toxic metal ions such as Pb^{2+} (Qiu et al., 2016; Su et al., 2013; Xiang and Lu, 2011), harmful food additives (Gu et al., 2015; Li et al., 2017) to disease markers (Su et al., 2012; Tang et al., 2016; Zhu et al., 2014). However, to the best of our knowledge, there is no report of PGM-based assays for the Ag^+ detection by far.

Herein, the PGM is used for the first time for portable quantitative readout of Ag^+ ions with the aid of a new type of μPADs, namely the 3D origami NM-μPADs. The μPAD construction is illustrated in Fig. 1. Each device is composed of a paper strip with hollow microstructures that are patterned by laser cutting (Nie et al., 2013) and a piece of circular polycarbonate NM loaded with 3,3′,5,5′-tetramethylbenzidine (TMB) (5 mm in diameter; as indicated by a yellow arrow in Fig. 1A). The patterned paper strip is designed with five folding layers (numbered from ***1*** to ***5***). Each layer contains a patterned function zone except the last layer. The layer ***5*** and the non-functional zones in the layers ***1*** to ***4*** are further hydrophobilized with wax (Zhang et al., 2014, Fig. 1C) for liquid-flow control. The function zone ***a*** (a 3.5 mm-diameter circular hole) in layer ***1***and the 5 mm-diameter circular function zone ***b*** in layer ***2*** are used for the sample addition and homogenization, respectively. The 5 mm-diameter circular zones ***c*** and ***d*** (located in the layers ***3*** and ***4***, respectively) are utilized for the immobilization and collection of glucose, respectively. After the TMB-loaded NM is sandwiched by the function zone ***b*** and the glucose-loaded zone ***c***, the paper strip is folded into a 3D origami device that is further fixed firmly with two clamps (Fig. 1B).

The detection principle of this instrument-free biosensing method is illustrated in Fig. 1C. After the sample solution is added onto the zone ***b***, the Ag^+ analytes flow to the zone ***c***, where the ions are reduced by the TMB loaded in the NM to form silver nanoparticle nuclei or seeds which in turn grow via more Ag^+-TMB redox reactions. The as-generated metal particles can block partial pores of the NM. As a result, a limited volume of solution flows through the NM to re-dissolve the glucose immobilized in the zone ***c***, some of which in turn flows to the zone ***d*** to be further collected for PGM measurement. The amount of the glucose recorded negatively relies on the Ag^+ level in the sample. The results demonstrate that the developed 3D NM-μPAD-based Ag^+ biosensors with PGM readout allow for simple, low-cost, and specific detection of analyte at picomolar levels within several minutes in artificial water samples as well as real water samples of pond water, tap water, drinking water and soil water.

2. Materials and methods

2.1. Materials and apparatus

3,3′,5,5′-tetramethylbenzidine (TMB) and phosphate-buffered saline (PBS, 10 mM, pH 5.6) solution were products of Sangon Biotechnology Co., Ltd. (Shanghai, China). Glucose, absolute ethyl alcohol, dimethylsulfoxide, silver nitrate ($AgNO_3$) and other metal salts were obtained from Xilong Chemical Co., Ltd. (Guangzhou, China). All other chemicals were also of analytical grade and used as received without further purification. The stock TMB solution (50 mM) was prepared in dimethylsulfoxide and diluted with absolute ethyl alcohol to specific levels before use. Unless otherwise specified, all stock and working solutions were prepared with deionized water with a specific resistivity of 18.2 MΩ cm that was produced from an ultrapure water system (UPS-II-20L) of Chengdu Yuechun Technology Co., Ltd. (Chengdu, China). The real water samples include commercially-available drinking water (a product of Hangzhou Wahaha Co., Ltd., Hangzhou, China), tap water obtained from our lab, pond water collected from a pond on our campus, and soil water that was collected from farmland around our campus.

Quantitative filter paper (~195 μm in thickness, ash ≤ 0.009%, ~1–3 μM in pore size and ~100 g cm^{-2} in average basis weight) was purchased from Hangzhou Xinhua Paper Industry Co., Ltd. (Hangzhou, China). Hydrophilic polycarbonate nanoporous membranes (NMs) (Whatman, ~50 nm in average pore size and ~3×10^8 pore cm^{-2} in average pore density; negligible absorption and adsorption of filtrate; autoclavable for 30 min at 121 °C) were the products of GE Healthcare Life Sciences. The personal glucose meter (PGM) was bought from Sannuo Biosensing Co., Ltd. (Changsha, China). Mini-type CO_2 laser cutting machine (XB-3020) was provided by Shangdong Xinbang Laser Equipment Co., Ltd. (Jinan, China). Reaction solutions were optically characterized by using an ultraviolet–visible spectrometer (Cary 50, Varian, USA). Meanwhile, morphology and element composition of the particles generated in these solutions were further characterized with a transmission electron microscope (TEM) that is equipped with energy-dispersive spectroscopy (EDS) (JEM-2100F, JEOL, Japan). Morphology characterization of the NMs used for analyzing a blank sample and an Ag^+ sample were carried out on an EDS-equipped scanning electron microscope (SEM, SU 5000, Hitachi, Japan).

2.2. Fabrication of reagent-loaded paper strips and NMs

The hollow microstructure-patterned paper strips were fabricated by a laser cutting method (Nie et al., 2013). As depicted in Fig. 1A, each paper strip consists of five continuous parts that serve as folding (independent) layers (numbered from ***1*** to ***5***). Except for layer ***5***, the four layers ***1–4*** contain patterned, specified circular function zones ***a*** – ***d***, respectively. The detailed sizes of its patterns (as illustrated in Fig. S1 in Supplementary Data) were designed as black lines on a white

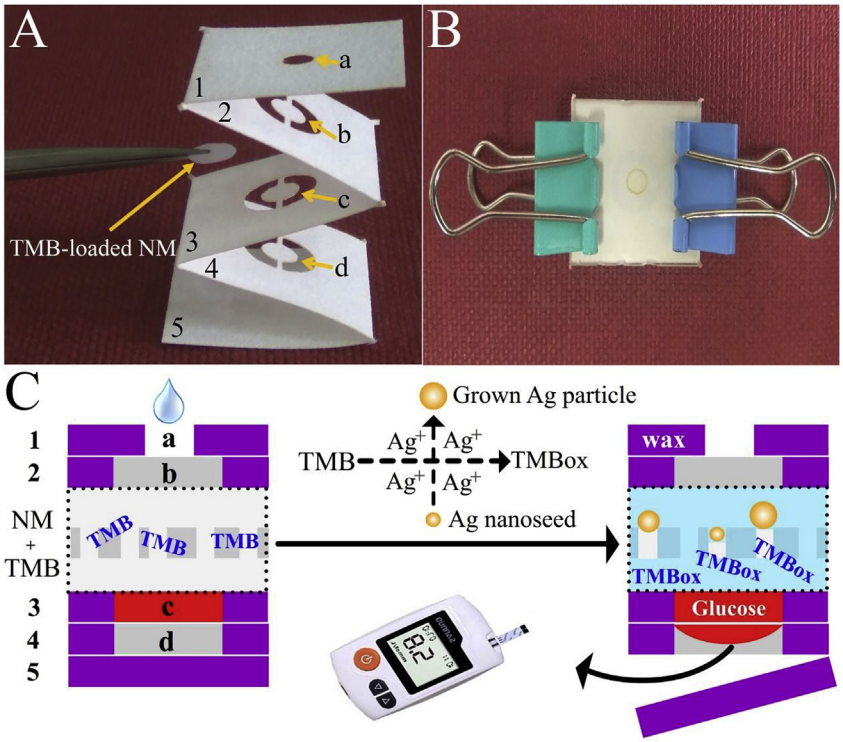

Fig. 1. (A) Construction of a 3D origami NM-μPAD. (B) Image of a 3D NM-μPAD that is fixed with two clamps and ready for use. (C) Schematical detection principle of the proposed instrument-free Ag^+ biosensor that combines analyte-triggered self-growing of silver nanoparticles to block the NM's pores for signal amplification with a portable personal glucose meter for quantitative readout.

background using CorelDraw X6. For the fabrication, the laser with a beam size of ~0.3 mm cut (pattern) a piece of filter paper laid flat on the working platform in the laser cutting machine. Its operation parameters include a laser wavelength of 10.64 μm, an applied current of 8.5 mA, a cutting rate of 20 mm s^{-1} and a laser power of 40 W. After laser patterning, the supporting (non-functional) zones in layers ***1–4*** and the whole layer ***5*** in the patterned strip were further hydrophobized by wax (Zhang et al., 2014). Moreover, 5 μL of a 600 mM glucose solution in 10 mM PBS (pH 5.6) was spotted on the circular function zone ***c*** in its layer ***3***, followed by air dry at room temperature. Then, the glucose-immobilized paper strip was folded into its 3D origami state (Fig. 1A). On the other hand, ~1.5 μL of a 10 mM TMB solution was deposited on a piece of 6 mm-diameter circular NM and allowed to air dry. Each freshly prepared 3D glucose-immobilized paper strip or TMB-loaded NM was stored in a sealed bag and kept away from light at room temperature. There is no significant loss of analytical sensitivity experimentally found during their storage period of one month. Packaging every reagent-immobilized 3D paper strip or NM individually via vacuum packaging technique could lead to the better storage stability.

2.3. Fabrication of 3D origami NM-μPADs for biosensing of Ag^+

In a typical Ag^+ assay, a 3D origami NM-μPAD was fabricated by sandwiching one piece of TMB-immobilized NM by the zones ***b*** and ***c*** in a folded glucose-loaded paper strip and further fixed firmly by two clamps (Fig. 1B). Then, a portion (10 μL) of Ag^+ sample solution (artificial sample in deionized water or real water sample) was added onto the zone ***b*** in the device's layer ***2***. Several minutes later, the two clamps were loosened, and a drop (10 μL) of PBS buffer (10 mM, pH 5.6) was introduced in the zone ***d*** of the layer ***4*** to suspend possible glucose products that flew from the zone ***c*** in the layer ***3*** for PGM measurement. Response signal of glucose concentration change ($\Delta C_{glucose}$) was defined as $\Delta C_{glucose} = C_b - C_s$, where C_b and C_s represent the glucose levels obtained from analysis of a blank sample (i.e., deionized water without analyte) and the Ag^+ sample, respectively. The $\Delta C_{glucose}$ value was used to estimate the Ag^+ level in the sample. Moreover, for a specificity study, a set of 3D NM-μPADs were adopted to detect other fifteen kinds of potential interfering metal ions (i.e., Fe^{3+}, Al^{3+}, Cr^{3+}, Zn^{2+}, Pb^{2+}, Ni^{2+}, Ca^{2+}, Fe^{2+}, Cd^{2+}, Co^{2+}, Cu^{2+}, Mg^{2+}, Hg^{2+}, Na^+, and K^+) in the same way.

3. Results and discussion

Herein, we propose a new paper-based method for the instrument-free quantitative detection of Ag^+. This method initially integrates analyte-triggered self-growing of Ag nanoparticles to block the NM's nanopores in 3D origami μPADs for rapid yet efficient signal amplification with a PGM as the portable quantitative reader (Fig. 1). It requires no experience and large desktop equipment. Moreover, its truly facile assay procedures could be completed by any nontechnical personnel within several minutes. These advantages would thus make this new method suitable for uses especially in resource-limited environments such as field-based water monitoring.

The core concept of our method focuses on the conversion of Ag^+ detection into glucose detection with the PGM, which relies on the analyte-triggered formation of metal nanoparticles that in turn adjust the glucose levels by blocking (closing) the nanopores in the NM-μPADs. Thus, the Ag^+-triggered the Ag^+-TMB redox reactions producing Ag nanoparticles in liquid-phase was first demonstrated. One can find from Fig. 2A that a freshly prepared TMB solution (2.5 mM) is clear and transparent (image a). Its ultraviolet–visible spectrum does not show any meaningful absorbance during a tested wavelength range from 330 to 800 nm (curve ***a*** in Fig. 2B). On the other hand, mixing the TMB solution with a 0.1 mM Ag^+ sample led to the formation of a blue mixture (image b in Fig. 2A). This should be attributed to the oxidation of TMB (TMBox) by Ag^+ (Gao et al., 2017; Lin et al., 2011; Song et al., 2010), which was further confirmed by three characteristic absorbance peaks recorded at 370, 458 and 659 nm (curve b in Fig. 2B). Actually, such a colour change from colourless to blue in the mixture as a result of the Ag^+-TMB redox reactions was very fast. It took place only within a few seconds (Fig. S2 in Supplementary Data).

The blue mixture solution was then characterized by TEM. Interestingly, as shown in its resulting microcosmic image (Fig. 2C), a

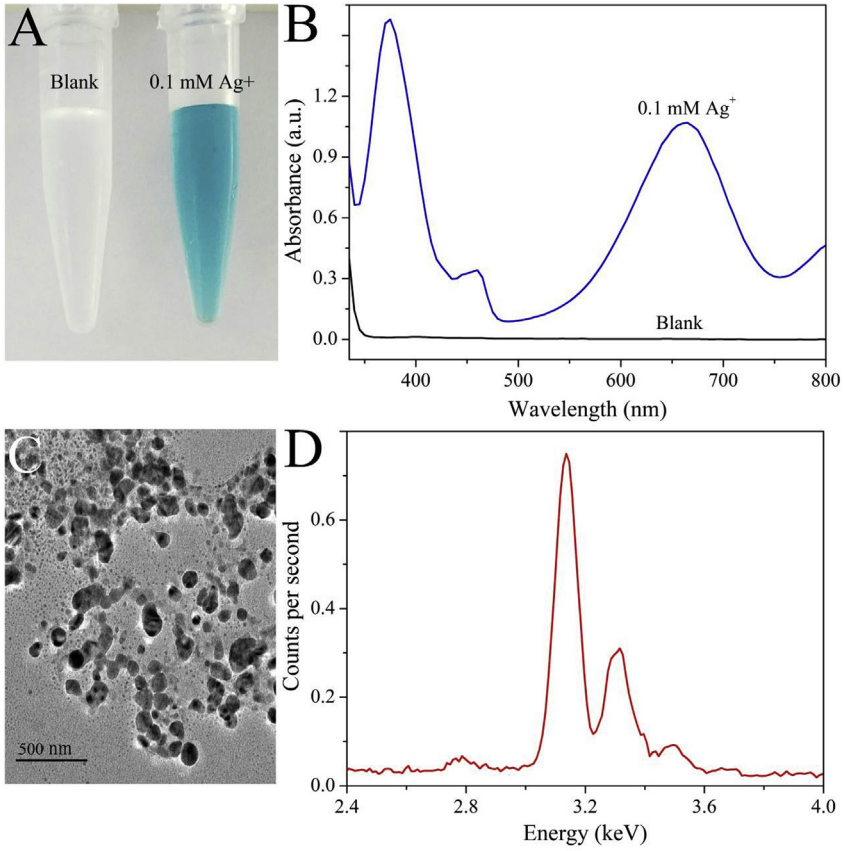

Fig. 2. (A) Image of two mixture solutions formed by mixing a 2.5 mM TMB solution separately with a blank sample (i.e., deionized water with analyte) and a 0.1 mM Ag^+ sample. (B) Ultraviolet–visible spectra of the two solutions shown in (A). (C) The TEM image and (D) corresponding EDS result obtained from the blue mixture shown in (A). (For interpretation of the references to colour in this figure legend, the reader is referred to the Web version of this article.)

great number of spherical nanoparticles with a diameter range of ~10–100 nm had been formed in the redox reactions between the TMB molecules and Ag^+ ions. The main elemental composition of these particles was subsequently proved to be silver by their EDS results (Fig. 2D). The two pieces of direct experimental evidence may be adopted to uncover a possible hypothesis or mechanism for the Ag^+-TMB redox reactions producing silver particles in situ. That is, Ag^+ ions would be reduced to zerovalent silvers assembling into small Ag nanoparticles as soon as the Ag^+ sample was mixed with the TMB solution (Yang et al., 2008). These small Ag particles further acted as nuclei (Wu et al., 2018) that allow more TMB molecules to reduce more Ag^+ ions to zerovalent Ag species. As a result, these small Ag seeds would grow up into bigger particles.

Next, the feasibility of generating Ag particles in situ blocking NM's pores to adjust Ag^+-dependent glucose levels in the NM-μPADs for PGM readout was studied. The first thing to consider is the glucose immobilization/collection efficiency in the paper body. In general, neither not all of the glucose molecules loaded on the zone ***c*** of a paper device could be carried to the zone ***d*** by a reaction solution that flows through the NM, or the glucose molecules adsorbed in the zone ***d*** could be totally collected from the paper body for a sequent PGM measurement. For this reason, one can find from Fig. 3A that a PGM value of ~33.1 mM glucose was obtained from a blank sample (i.e., water without Ag^+) while using a glucose concentration up to 600 mM for its immobilization in zone ***c***. Higher glucose levels would lead to no signal output as the measurable glucose levels of the PGM used herein range from 1.1 to 33.3 mM (Fig. S3 in Supplementary Data). In contrast, for 64 nM Ag^+, a glucose concentration as low as ~1.1 mM was recorded on the PGM.

In order to understand such a dramatic difference in PGM signals, the surface morphologies of a piece of NM unused and those utilized in the two cases were contrastively characterized with SEM and EDS techniques. It was obviously shown in Fig. 3B that there are a large number of circular pores with an average diameter of ~50 nm distributed in the unused NM. Moreover, almost no changes were observed in the microscopic morphology of the NM used for the assay of a blank sample (Fig. 3C). In other words, in comparison with that of the unused one (Fig. 3B), almost all of its nanopores kept their original "open" states, which surely facilitated the reaction solution flowing to redissolve and carry a substantial level of glucose loaded in zone ***c*** to zone ***d*** for PGM detection (Fig. 3A). On the other hand, as expected, a more smooth NM was obtained in the case of assaying a 0.1 mM Ag^+ sample, as most of its pores had been filled ("closed") with lots of Ag particles created via more Ag^+-TMB redox reactions (Fig. 3D). Thus, only a small volume of reaction solution could flow through the NM to zone ***c*** for redissolving the glucose immobilized. As a result, a quite low level of glucose was collected from zone ***d***, leading to a very small PGM signal.

After demonstrating the feasibility of in-situ formation of Ag particles in liquid phase or on the NM surface and the PGM readout of Ag^+-dependent glucose level on 3D NM-μPADs, the specificity of the proposed method was then evaluated. More specifically, a set of paper devices were utilized to assay fifteen kinds of potential interfering metal ions in water (i.e., Fe^{3+}, Al^{3+}, Cr^{3+}, Zn^{2+}, Pb^{2+}, Ni^{2+}, Ca^{2+}, Fe^{2+}, Cd^{2+}, Co^{2+}, Cu^{2+}, Mg^{2+}, Hg^{2+}, Na^+, and K^+; 2.4 μM each), comparing with the results of analyzing a blank sample without the analyte and a 64 nM Ag^+ sample. The $C_{glucose}$ results measured by the same PGM are shown in Fig. 4A. It clearly shows that similar $C_{glucose}$ values as large as ~32.3 mM were obtained for these non-specific ions. And no significant differences were observed between their PGM responses and that recorded from the blank sample (~32.9 mM). In contrast, a small $C_{glucose}$ value as low as ~1.1 mM was measured for the Ag^+ assay, although its level is far lower than that of the chosen non-specific ions. The data indicates that this new Ag^+ assay possesses good detection specificity. This is presumably due to that only the Ag^+ ions could trigger the nucleating and growing of Ag particles on the solid NM integrated into the used device to efficiently block (close) its nanopores

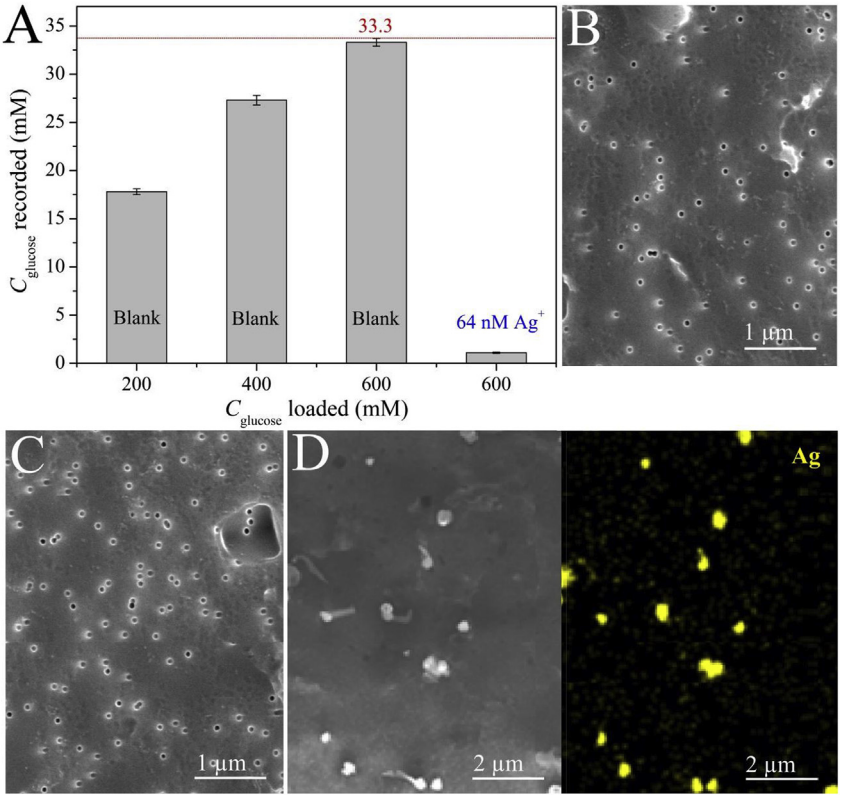

Fig. 3. (A) Glucose concentrations ($C_{glucose}$) recorded by PGM for assays of the blank sample (deionized water with Ag^+) and a 64 nM Ag^+ sample using μPADs loaded with different $C_{glucose}$. Each data point is an average of three replicates and error bars indicate standard deviations. SEM images of original NMs (B) and these used for a blank sample (C) and a 0.1 mM Ag^+ sample (D), respectively. The right part of (D) shows the corresponding EDS result (image) obtained from the Ag^+ assay.

(Anderson et al., 2017).

The main experimental factors for Ag^+ detection were studied in detail, including the concentration of glucose deposited on zone ***c***, the concentration and volume of TMB spotted on each piece of NM, the volume of sample consumed in one assay run, and the time required for the reactions took place in every 3D NM-μPAD (Figs. S4–S7 in Supplementary Data). Then, in order to evaluate the sensitivity and robustness of this new method, a series of artificial water samples with varying Ag^+ concentrations ranging from 0 to 64 nM were analyzed under the resulting optimized factors. The relationship between the $C_{glucose}$ values recorded by the same PGM and the Ag^+ concentrations (C_{Ag+}) tested is displayed in Fig. 4B. It is clearly observed from Fig. 4B that as the Ag^+ concentration increases, the $C_{glucose}$ values decreases, presenting negative analyte level-dependent $C_{glucose}$ responses. Interestingly, as further shown in the inset of Fig. 4B, the calibration curve that describes the relationship between the $\Delta C_{glucose}$ values and the logarithm values of Ag^+ concentrations ($LogC_{Ag+}$) has two linear sections. It can be described by the regression equation $\Delta C_{glucose}$ (mM) = 5.7343 $LogC_{Ag+}$ + 7.3881 (R = 0.9933) for the 62.5 pM to 8 nM Ag^+ concentration range and the equation $\Delta C_{glucose}$ (mM) = 23.0633 $LogC_{Ag+}$ - 9.3817 (R = 0.9561) for the 8–50 nM range. The limit of detection (LOD) for Ag^+ was estimated to be ~58.1 pM using the first equation according to the 3σ rule. The occurrence of two linear concentration ranges (LCR) might be attributed to the different growing rates of Ag^+ nanoparticles at low and high Ag^+ levels in the NM's nanopores. However, the exact mechanism still needs more investigation to achieve a definite conclusion. In comparison with some recent fluorescence, absorbance, or electrochemistry methods for Ag^+

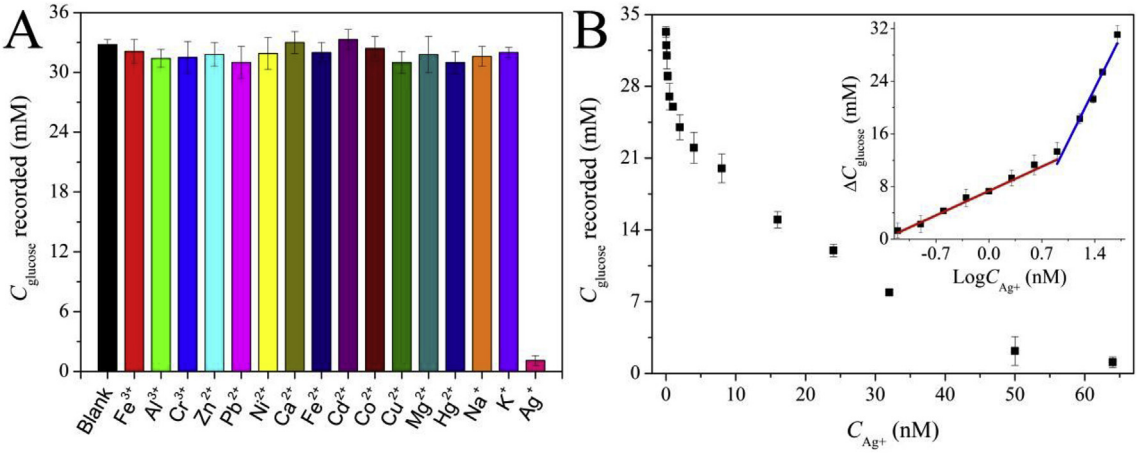

Fig. 4. (A) Results of glucose concentrations ($C_{glucose}$) recorded from the blank sample and different metal ions: Ag^+, 64 nM; other ions, 2.4 μM. (B) $C_{glucose}$ values recorded for detection of various concentrations of Ag^+ samples. An inset shows the calibration curve that describes the relationship between the $C_{glucose}$ value changes ($\Delta C_{glucose}$) and the logarithm values of Ag^+ concentrations ($LogC_{Ag+}$). Each data point is an average of three replicates and error bars indicate standard deviations.

Table 1
Performance comparison of this new method with some other quantitative Ag^+ assays.

Quantitative method	LCR[a]	LOD[b]	Portable	Cost	Assay time (min)	References
Surface plasmon resonance	0.05–2 μM	10 nM	No	Very high	45	Chang et al. (2012)
Fluorescence	3–300 nM	1.5 nM	No	High	30	Chen et al. (2013)
Fluorescence	0.02–1.5 μM	14 nM	No	High	10	Xie et al. (2012)
Absorbance	0.1 nM–10 μM	80 pM	No	High	6	Gao et al. (2017)
Absorbance	5–40 μM	1 μM	No	High	90	He et al. (2016)
Absorbance	1–170 μM	1 μM	No	High	10	Liu et al. (2013)
Absorbance	0.1–1 μM	48.6 nM	No	High	120	Wang et al. (2013)
Absorbance	0.4–1 μM	100 nM	No	High	5	Lin et al. (2010)
Absorbance	0.05.3 μM	64 nM	No	High	110	Zhou et al. (2010)
Electrochemistry	1 pM–100 nM	0.47 pM	No	High	120	Miao et al. (2013)
Electrochemistry	0.1–0.8 μM	10 nM	No	High	120	Lin et al. (2011)
μPAD with PGM	0.0625–8 nM; 8–50 nM	58.1 pM[c]	Yes	Very low	7	This work

[a] LCR, linear concentration range.
[b] LOD, limit of detection.
[c] The LOD of 58.1 pM of this work was estimated using the regression equation obtained from the LCR of 0.0625.8 nM according to the 3σ rule.

detection (Table 1), this 3D NM-μPAD-based strategy needs just a ubiquitous PGM (rather than any bulky equipment) for a portable quantitative readout. In particular, it can not only be operated by unskilled personnel to rapidly achieve comparable or even better sensitivity but also offers a useful potential capability for POCT applications (Table 1). Moreover, the average relative standard deviation (RSD) in three repetitive assays of the tested Ag^+ samples was ~6.41%, suggesting an acceptable reproducibility of the new approach. The major source of detection variations might be the manual operations for the immobilization of TMB (in the NM) and glucose (in the device's zone ***c***) under the open ambient conditions including temperature and humidity. Better detection reproducibility could be expected if more precise reagent immobilization would be performed in constant experimental conditions.

With these good results above in hand, the accuracy and practicability of this new assay method were additionally assessed by carrying out recovery tests of several real water samples according to the same procedures. The real water samples include the commercially available drinking water, tap water obtained from our lab, pond water collected from a pond on our campus, and soil water that was collected from farmland around our campus. It should be pointed out that all of these water samples should be filtrated with NMs to remove potential interferences before their analysis. Then, six parallel experiments for each sample were performed. As shown in Table 2, the recovery results obtained from these tests range from 93.02 to 107.0% and the RSDs are between 4.65 and 10.0% (n = 6). The acceptable recovery percentages and small standard deviations thus validate relatively high accuracy and practicability of the new method for specifically identifying and quantifying Ag^+ ions in real complex matrices including environmental water.

Table 2
Recovery of Ag^+ in several real water samples.

Real sample	Found[a] (nM)	Added (nM)	Calculated[b] (nM)	Recovery (%)	RSD[c] (%, n = 6)
Drinking water	0.00	8.00	7.53	106.2	8.99
	0.00	16.0	16.2	98.77	9.80
	0.00	32.0	33.4	95.81	9.13
Tap water	0.00	8.00	7.92	101.0	5.82
	0.00	16.0	16.1	99.38	10.0
	0.00	32.0	29.9	107.0	9.23
Pond water	0.00	8.00	8.51	94.01	7.77
	0.00	16.0	17.2	93.02	7.99
	0.00	32.0	33.9	94.40	9.22
Soil water	0.00	8.00	8.59	93.13	10.0
	0.00	16.0	14.9	107.3	4.65
	0.00	32.0	32.1	99.69	9.35

[a] The original Ag^+ concentrations in the samples detected using atomic absorption spectroscopy.
[b] The total Ag^+ concentrations in the samples determined using the proposed method.
[c] RSD, relative standard deviations.

4. Conclusion

We have successfully developed a new type of 3D origami μPADs that integrate NMs with PGMs for specific biosensing detection of picomolar Ag^+ ions. The analyte-triggered self-growing of Ag particles in the NMs of μPADs could allow for rapid yet efficient signal amplification. The battery-powered and handheld PGM is cheap and widely accessible and proves easy-to-use for sensitive and portable quantitative measurement. Such a 3D NM-μPAD-based biosensor with PGM readout has been well demonstrated to achieve a comparable or even better performance in comparison with most of existing Ag^+ assays, in terms of portability, sensitivity, technical requirements and assay time. This universal instrument-free biosensing platform could offer new opportunities for constructing various POCT systems for uses particularly in resource-poor settings, such as field-based and household analysis.

Future work would focus on: (1) improvement of the overall design of the 3D origami NM-μPADs proposed for realizing practical POCT applications for Ag^+; (2) enhancement of their detection limits and linear ranges by seeking another type of NMs and/or additional co-reaction reagents that are more sensitive to the amount of nanoparticles formed per nanopore; and (3) development of equipment-free biosensing methods with the 3D NM-μPADs and PGMs for other targets that make the use of new reaction chemistries for adjusting the liquid flowing in NM's pores.

Declaration of interests

The authors declare that they have no known competing financial interests or personal relationships that could have appeared to influence the work reported in this paper.

The authors declare the following financial interests/personal relationships which may be considered as potential competing interests:

CRediT authorship contribution statement

Wencheng Xiao: Conceptualization, Data curation. **Yiming Gao:** Data curation. **Yun Zhang:** Funding acquisition, Project administration, Writing - original draft. **Jiao Li:** Formal analysis. **Zhaoying Liu:** Software. **Jinfang Nie:** Resources, Writing - review & editing. **Jianping Li:** Formal analysis.

Acknowledgements

The authors gratefully acknowledge the financial support from National Science Foundation of China (Nos. 21765007, 21565012, 21365009 and 21874032), Guangxi Key Research Project (No. GuikeAB17129003), Guangxi Science Fund for Distinguished Young Scholars (2018GXNSFFA281002), and Open Foundation of Guangxi Key Laboratory of Electrochemical and Magnetochemical Functional Materials (No. EMFM20181120).

Appendix A. Supplementary data

Supplementary data to this article can be found online at https://doi.org/10.1016/j.bios.2019.05.003.

References

Anderson, K., Poulter, B., Dudgeon, J., Li, S.E., Ma, X., 2017. Sensors 17, 18071–180711.
Alizadeh, A., Khodaei, M.M., Hamidi, Z., Shamsuddin, M., 2014. Sens. Actuators B-Chem. 190, 782–791.
Chang, C.C., Lin, S., Wei, S.C., Yu, C.S., Lin, C.W., 2012. Anal. Bioanal. Chem. 402 (9), 2827–2835.
Chen, P.C., Yeh, T.Y., Ou, C.M., Shih, C.C., Chang, H.T., 2013. Nanoscale 5 (11), 4691–4695.
Chen, Y.J., Liu, C.Y., Tsai, D.Y., Yeh, Y.C., 2018. Sens. Actuators B-Chem. 259, 784–788.
Choi, S., Lee, G., Park, I.S., Son, M., Kim, W., Lee, H., Lee, S.Y., Na, S., Yoon, D.S., Bashir, R., 2016. Anal. Chem. 88 (22), 10867–10875.
Dai, B., Cao, M., Fang, G., Liu, B., Dong, X., Pan, M., Wang, S., 2012. J. Hazard Mater. 219–220 (6), 103–110.
Drake, P.L., Hazelwood, K.J., 2005. Ann. Occup. Hyg. 49 (7), 575–585.
Gao, Z., Liu, G.G., Ye, H., Rauschendorfer, R., Tang, D., Xia, X., 2017. Anal. Chem. 89 (6), 3622–3629.
Gu, C., Lan, T., Shi, H.C., Lu, Y., 2015. Anal. Chem. 87 (15), 7676–7682.
Gumpu, M.B., Sethuraman, S., Krishnan, U.M., Rayappan, J.B.B., 2015. Sensor. Actuator. B Chem. 213 (3), 515–533.
Hadrup, N., Lam, H.R., 2014. Regul. Toxicol. Pharmacol. 68 (1), 1–7.
He, Y., Liang, Y., Song, H., 2016. Plasmonics 11 (2), 587–591.
Hossain, S.M.Z., Brennan, J.D., 2011. Anal. Chem. 83 (22), 8772–8778.
Hossain, Z., Huq, F., 2002. J. Inorg. Biochem. 90 (3), 85–96.
Kumar, M., Kumar, R., Bhalla, V., 2011. Org. Lett. 13 (3), 366–369.
Li, F., Zhang, R., Kang, H., Hu, Y., Liu, Y., Zhu, J., 2017. Anal. Methods 9 (46), 6507–6512.
Lin, C.Y., Yu, C.J., Lin, Y.H., Tseng, W.L., 2010. Anal. Chem. 82 (16), 6830–6837.
Lin, Y., Gritsenko, D., Feng, S., Teh, Y.C., Lu, X., Xu, J., 2016. Biosens. Bioelectron. 83, 256–266.
Lin, Z., Li, X., Kraatz, H.B., 2011. Anal. Chem. 83 (17), 6896–6901.
Liu, B., Tan, H., Chen, Y., 2013. Microchim. Acta 180 (5–6), 331–339.
Liu, L., Lin, H.W., 2014. Anal. Chem 86, 8829–8834.
Martinez, A.W., Phillips, S.T., Butte, M.J., Whitesides, G.M., 2007. Angew. Chem. Int. Ed. 46 (8), 1318–1320.
Mensah, S.T., Gonzalez, Y., Calvo-Marzal, P., Chumbimuni-Torres, K.Y., 2014. Anal. Chem. 86 (15), 7269–7273.
Miao, P., Ning, L., Li, X., 2013. Anal. Chem. 85 (16), 7966–7970.
Morbioli, G.G., Mazzu-Nascimento, T., Stockton, A.M., Carrilho, E., 2017. Anal. Chim. Acta 970, 1–22.
Nie, J., Liang, Y., Zhang, Y., Le, S., Li, D., Zhang, S., 2013. Analyst 138 (2), 671–676.
Nie, J.F., Zhang, Y., Lin, L.W., Zhou, C.B., Li, S.H., Zhang, L.M., Li, J.P., 2012. Anal. Chem. 84 (15), 6331–6335.
Qiu, Z., Shu, J., Jin, G., Xu, M., Wei, Q., Chen, G., Tang, D., 2016. Biosens. Bioelectron. 77, 681–686.
Ratte, H.T., 1999. Environ. Toxicol. Chem. 18 (1), 89–108.
Song, Y., Qu, K., Zhao, C., Ren, J., Qu, X., 2010. Adv. Mater. 22 (19), 2206–2210.
Su, J., Xu, J., Chen, Y., Xiang, Y., Yuan, R., Chai, Y., 2012. Chem. Commun. 48 (55), 6909–6911.
Su, J., Xu, J., Chen, Y., Xiang, Y., Yuan, R., Chai, Y., 2013. Biosens. Bioelectron. 45 (14), 219–222.
Tang, J., Huang, Y., Liu, H., Zhang, C., Tang, D., 2016. Biosens. Bioelectron. 79, 508–514.
Trindade, A.S.N., Dantas, A.F., Lima, D.C., Ferreiraa, S.L.C., Teixeira, L.S.G., 2015. Food Chem. 185, 145–150.
Upadhyay, P.K., Marpu, S.B., Benton, E.N., Williams, C.L., Telang, A., Omary, M.A., 2018. Anal. Chem. 90, 4999–5006.
Wang, F., Wu, Y., Zhan, S., He, L., Zhi, W., Zhou, X., Zhou, P., 2013. Aust. J. Chem. 66 (1), 113–118.
Wang, H., Wu, Z., Chen, B., He, M., Hu, B., 2015. Analyst 140, 5619–5626.
Wu, D., Hu, N., Liu, J.C., Fan, G.S., Li, X.T., Sun, J., Dai, C.J., Suo, Y.R., Lia, G.L., Wu, Y.N., 2018. Talanta 190, 103–109.
Xia, Y., Si, J., Li, Z., 2016. Biosens. Bioelectron. 77, 774–789.
Xiang, Y., Lu, Y., 2011. Nat. Chem. 3 (9), 697–703.
Xiang, Y., Lu, Y., 2012. Anal. Chem. 84 (4), 1975–1980.
Xie, W.Y., Huang, W.T., Li, N.B., Luo, H.Q., 2012. Chem. Commun. 48 (1), 82–84.
Yamada, K., Henares, T.G., Suzuki, K., Citterio, D., 2015. Angew. Chem. Int. Ed. 54 (18), 5294–5310.
Yang, J., Wang, H., Zhang, H., 2008. J. Phys. Chem. C 112 (34), 13065–13069.
Yang, X., Wang, E., 2011. Anal. Chem. 83 (12), 5005–5011.
Yang, Y., Noviana, E., Nguyen, M.P., Geiss, B.J., Dandy, D.S., Henry, C.S., 2016. Anal. Chem. 89 (1), 71–91.
Zhang, Y., Gao, D., Fan, J., Nie, J., Le, S., Zhu, W., Yang, J., Li, J., 2016. Biosens. Bioelectron. 78, 538–546.
Zhang, Y., Zhou, C., Nie, J., Le, S., Qin, Q., Liu, F., Li, Y., Li, J., 2014. Anal. Chem. 86 (4), 2005–2012.
Zhou, X.H., Kong, D.M., Shen, H.X., 2010. Anal. Chem. 82 (3), 789–793.
Zhu, X., Xu, H., Lin, R., Yang, G., Lin, Z., Chen, G., 2014. Chem. Commun. 50 (58), 7897–7899.